PROCEEDINGS OF SCIENCE

Update on the performance of the MAGIC Intensity Interferometer

Irene Jiménez Martínez,[a,*] **V. A. Acciari,**[b] **A. Cifuentes,**[a] **E. Colombo,**[b] **J. Cortina,**[a] **C. Delgado,**[a] **C. Díaz,**[a] **M. Fiori,**[c] **D. Fink,**[d] **D. Guberman,**[f] **T. Hassan,**[a] **E. Lyard,**[e] **M. Mariotti,**[c] **G. Martínez,**[a] **R. Mirzoyan,**[d] **G. Naletto,**[c] **T. Njoh Ekoume,**[b] **M. Polo,**[a] **N. Produit,**[e] **J. J. Rodríguez-Vázquez,**[a] **P. Saha,**[g] **T. Schweizer,**[d] **R. Walter,**[e] **C.W. Wunderlich,**[f] **L. Zampieri**[c] **and for the MAGIC collaboration**

[a] *CIEMAT, Avda. Complutense, 40, Madrid, Spain*
[b] *IAC, E-38200 La Laguna, Spain*
[c] *Università di Padova, I-35131 Padova, Italy*
[d] *Max-Planck-Institut für Physik, D-80805, Munich, Germany*
[e] *Observatoire Astronomique de Genève, CH-1290 Versoix, Switzerland*
[f] *Università di Pisa and INFN Pisa, I-56126 Pisa, Italy*
[g] *Physik-Institut, University of Zurich, Zurich, Switzerland*

E-mail: irene.jimenez@ciemat.es

In recent years, the MAGIC telescopes have been equipped with a setup that allows its Imaging Atmospheric Cherenkov Telescopes (IACTs) to function as an Intensity Interferometer. The deadtime-free setup includes a 4-channel GPU-based real-time correlator together with optical filters in the 350-450 nm wavelength range and specialized Active Mirror Control (AMC) configurations. This implementation allows MAGIC to perform measurements of the spatial coherence (visibility) of the intensity fluctuations of an object's starlight over several separations (baselines) and construct a model of said object. The accessible baseline range for MAGIC is 40-90 m which translates into an angular resolution of 0.5-1 mas. Additionally, thanks to the AMC it can access even smaller baselines, of less than 17 m (which is the diameter of each of both dishes) to measure objects of greater angular size (>1 mas) and even measure the zero-baseline correlation, which is key to calibrate the system. We present the latest measurements that allow us to understand the performance and systematics of our setup and validate our analysis.

38th International Cosmic Ray Conference (ICRC2023)
26 July - 3 August, 2023
Nagoya, Japan

*Speaker

PoS(ICRC2023)728

1. Introduction

Between 1964 and 1972, R. Handbury Brown et al. measured the diameter of 32 stars using the intensity interferometry technique [6] with two telescopes very similar to current IACTs. The technique was abandoned due to the lack of fast photo-sensors and telescopes with the large collection area needed to overcome the ∼1 kHz atmospheric turbulence. The technique resurfaced in 2019, when major IACT observatories like VERITAS [1], MAGIC [2] and later HESS started to exploit their IACT arrays as optical intensity interferometers, showing a significant boost in sensitivity.

The intensity interferometry technique is based on the concept that an extended object of angular size θ formed by many incoherent emitting sources produces a speckled wavefront at the position of the observer with a typical size λ/θ, where λ is the wavelength [5]. For a pair of observers separated by a distance much smaller than that typical size (λ/θ) it is very likely that they are within the same speckle and therefore observe the same intensity fluctuations, i.e. they see correlated fluctuations. Additionally, the Van Cittert-Zernike theorem states that when observing a thermal light source through a narrow spectral band ($\delta\lambda/\lambda_0 \ll 1$), the coherence of light between two points is proportional to the Fourier transform of the intensity profile of the source at said distance. For non-polarized light it can be shown that:

$$g^{(2)}_{1,2} = \frac{\langle I_1(t) \cdot I_2(t+\tau)\rangle_t}{\langle I_1(t)\rangle \cdot \langle I_2(t+\tau)\rangle_t} = 1 + \frac{\Delta f}{\Delta \nu} \cdot |V_{1,2}(\tau)|^2 \tag{1}$$

where $g^{(2)}_{1,2}$ is the second-order intensity correlation function, $I_i(t)$ is the intensity of light at the detector i (1 or 2) at time t, τ is the time delay due to the difference in optical path, $\langle x\rangle_t$ represents the time average of x, Δf where $\Delta f << \Delta\nu$ is the electronic bandwidth, $\Delta\nu$ is the optical bandwidth and $V_{1,2}(\tau)$ is the normalized degree of first-order mutual coherence of the light at the delay τ, also called visibility. Measuring the visibility over a set of different delays or baselines provides morphological information about the thermal emission of the source, which is a valuable tool in a broad range of stellar science cases. Nevertheless, it is useful to note that between two detectors only the modulus of the complex visibility is measured and therefore the phase information is lost, making it impossible to perform imaging of the source.

The modulus of the complex visibility function $|V_{1,2}(\tau)|$ can take different shapes depending on the light profile of the source. For example, in the case of an uniformly illuminated disk the expression would be:

$$|V_{1,2}| = 2 \cdot \frac{J_1(\pi \cdot d_{1,2} \cdot \theta/\lambda)}{\pi \cdot d_{1,2} \cdot \theta/\lambda} \tag{2}$$

where J_1 is the Bessel function of the first kind, $d_{1,2}$ is the baseline between the detectors, θ is the angular size of the equivalent uniform disc and λ is the effective wavelength. But there are other cases in which there is no radial symmetry, and the expression is more complex, like for fast-rotators (stars that spin so rapidly they become elongated in the perpendicular direction of the rotation axis) and multiple systems (like spectroscopic binaries, if they are close enough and have the right size, their intensity patterns intertwine).

2. The MAGIC Stellar Intensity Interferometer

The MAGIC telescopes are a system of two IACTs of 17 m mirror dish diameter, located at an elevation of 2200 m above sea level, at the Roque de los Muchachos Observatory in La Palma, Canary Islands (Spain). MAGIC provides an integral sensitivity of 0.66 ± 0.03 % of the Crab Nebula flux above 220 GeV in 50 h of observation, and allows the measurement of photons in the energy range from 50 GeV to above 50 TeV [4].

The main objective for IACTs, such as the MAGIC telescopes, is to observe the gamma-ray night-sky. Gamma-rays do not pass through our atmosphere but they interact with it, producing Extensive Atmospheric Showers (EAS) that emit faint fast blue flashes of Cherenkov light. By characterizing the intensity and the spatial and temporal pattern of this light, one can study different properties of the primary: its nature (gamma photons or otherwise), its direction (the astronomical source) and its energy (to reconstruct their spectrum). In order to perform this kind of observations, IACTs make use of several technical features that make them incidentally well suited for intensity interferometry observations: they come in groups (each combination of telescopes is a different baseline), they have time resolution of nanoseconds (needed to resolve the correlation peak), they are sensitive to single photo-electrons (and therefore coherence of individual photons) and they have large reflective mirrors (more photons means more statistics and better S/N).

In recent years, the MAGIC telescopes have undergone several technical modifications ([2, 7, 8]) like the implementation of a digitizer and GPU-based real-time correlator, special configuration of its AMC (to focus the light to the infinite instead of the typical altitude of EAS of 10 km and to concentrate it into just one or two photo-multipliers or PMTs) and the automatic deployment of optical filters using the target holder, that allow the system to transform into an intensity interferometer in less than a minute and then back to Very High Energy (VHE, E>100 GeV) observations just as quickly (useful for transients). This makes MAGIC Intensity Interferometer an extremely high duty cycle instrument, having taken more than 500 hours of observations since 2021. Said observations were mainly performed during Moon breaks, which are periods with bright Moon-light conditions in which IACTs cannot perform sensitive VHE observations, but the intensity interferometer can, thanks to the optical filters that greatly reduce the amount of blue Moon-light that gets into the PMT.

3. Methodology

Each telescope's target holder has installed three Semrock 425-26 nm optical filters as can be seen in Figure 1 (left) of [8]. When the target holder is deployed, each filter falls in front of one of the three PMTs (pixels): two are used for measuring correlations and one is for keeping track of background light.

Measuring our signals using the same kind of PMTs that we use for VHE observations means that the signal we are measuring is not DC coupled, so we are not measuring the signal intensities directly I_i but the anode currents of the PMTs which are proportional to them $\langle I_i \rangle \propto DC_i$. Since the intensity fluctuations follow a Poisson distribution, it can be shown as well that $\sqrt{\langle (I_i(t) - \langle I_i \rangle)^2 \rangle} \propto \sqrt{DC_i}$.

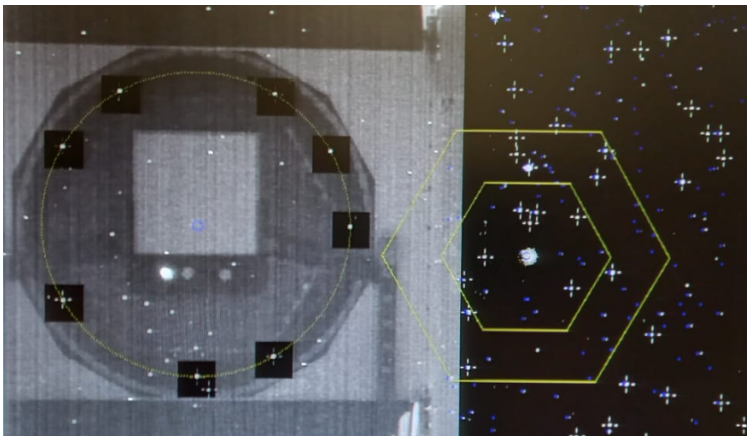

Figure 1: Picture of one of MAGIC cameras during an intensity interferometry observation. The light from the target star, which can be seen within the yellow hexagons on the right, is focused by the AMC into one of the holes with filters in the target holder (left hole), while the other holes are illuminated by diffuse background light (right holes).

Camera reports are produced every second, keeping track of the DCs and other parameters, while the signal from the pixels is digitized at $500{\cdot}10^6$ Samples/s. The digitized signal is later processed by the GPU-correlator which computes the Pearson's correlation:

$$\rho(\tau) = \frac{\langle (I_1(t) - \langle I_1 \rangle) \cdot (I_2(t+\tau) - \langle I_2 \rangle) \rangle}{\sqrt{\langle (I_1(t) - \langle I_1 \rangle)^2 \rangle} \sqrt{\langle (I_2(t+\tau) - \langle I_2 \rangle)^2 \rangle}} \tag{3}$$

We correct for the time delay coming from the hardware setup, which is different for each pixel due to different lengths of the optical fibers, and the additional delay coming from the different optical paths between the telescopes when tracking the source at different zenith/azimuth positions. We apply a 12 MHz frequency high-pass filter to remove slow residual noise, and then we extract the amplitude of the cross-correlation signal at 0 ns delay as the value of the Pearson's correlation. Finally, we take said value and correct it by the DCs to calculate the contrast, which is proportional to the modulus of the complex visibility:

$$c(\tau) = \frac{\langle (I_1(t) - \langle I_1 \rangle) \cdot (I_2(t+\tau) - \langle I_2 \rangle) \rangle}{\langle I_1(t) \rangle \cdot \langle I_2(t+\tau) \rangle_t} = K \cdot \frac{\rho \beta \sqrt{G_1 G_2}}{\sqrt{DC_{1,Star} DC_{2,Star}}} \tag{4}$$

where K is a setup constant, G_i are the gains of the PMTs, $DC_{i,Star}$ are the DCs of the pixels for which the starlight has been focused into and β is the ratio between the light coming from the night-sky background (NSB) and the star:

$$\beta = \sqrt{\frac{(DC_{1,Star} + DC_{1,NSB})(DC_{2,Star} + DC_{2,NSB})}{DC_{1,Star} DC_{2,Star}}} \tag{5}$$

The contrast can be normalized in order to calculate the visibility:

$$c(d) = g^{(2)}_{1,2} - 1 = \frac{\Delta f}{\Delta \nu} \cdot |V_{1,2}(d)|^2 \rightarrow \frac{c(d)}{c(0)} = |V_{1,2}(d)|^2 \tag{6}$$

where $c(0)$ is a correlation normalization factor, also called zero-baseline correlation (ZBC), and it is the value that the correlation takes at baseline 0 or in other words, the correlation that would be measured for a point-like source. There are several ways to estimate or directly measure its value that can be found in [8]. This value together with measurements of the correlations at different time delays or baselines (and different u-v plane coordinates for cases without radial symmetry) can be used to reconstruct the brightness distribution of the thermal emission of the source.

The value of the ZBC is expected to be constant for each pixel pair, but several scenarios are described in the next section that can affect its value over short and long periods of time.

4. Systematics evaluation

The MAGIC Collaboration carefully evaluated the main systematics affecting their VHE gamma-ray analysis [3, 4]. Given the very different nature of the measurement, these systematics actually do not affect interferometry observations the same way. For instance, the uncertainty in the amount of light detected by IACTs mainly affects S/N (see [5]), but does not add as a systematic.

But there are factors that can change not only the S/N of the correlation signal, but also the ZBC (which could lead to a wrong calibration of the setup and a wrong calculation of the visibility). We have performed an extensive study of the effects that can and can not add systematic uncertainties to our intensity interferometry analysis.

Some effects that do not add systematic uncertainty are: the amount of light that hits the PMTs (provided that the stored DC values properly account for the average photon flux that reaches the PMTs) and the gain evolution of components after DC/ADC branch (Pearson's correlation needs to be unit-less and so does the visibility, so changes in gain coming from the vertical cavity surface emitting lasers (VCSels) or any component after the DC/ADC branch cancel out when we calibrate our measured correlation with the average photon fluxes (see Eq. 4)).

4.1 Electronic bandwidth

While the single photo-electron response of the PMTs is fairly stable, the VCSels' signal transmission could change in short timescales, producing a time-dependent variation of the electronic bandwidth. Thanks to the versatility of the GPU correlator, we are able to compute the auto-correlation simultaneously to the cross-correlation. This means that we can keep track of the electronic bandwidth of each channel (pixel) over time. Our measurements represented in Figure 4 show that for values of photon flux (which is proportional to the measured DC counts) higher than a certain threshold, the width of the auto-correlation signal, and therefore the electronic bandwidth, remains constant (less than 1% deviation for all pixels). This is because for lower photon fluxes the signal is dominated by electronic noise, but for higher fluxes it follows a poissonian.

4.2 Optical bandwidth

The distribution of photons that pass through the narrow-band filters has a certain QE ($\alpha(\lambda_0)$) but this factor is affected by the angle of incidence (AOI) of the photons that reach them. Simulations of AOIs up to 26 deg (which is the cut-off angle of the Winston cones in front of every PMT) show how this affects the shape of the optical band-pass in Figure 3.

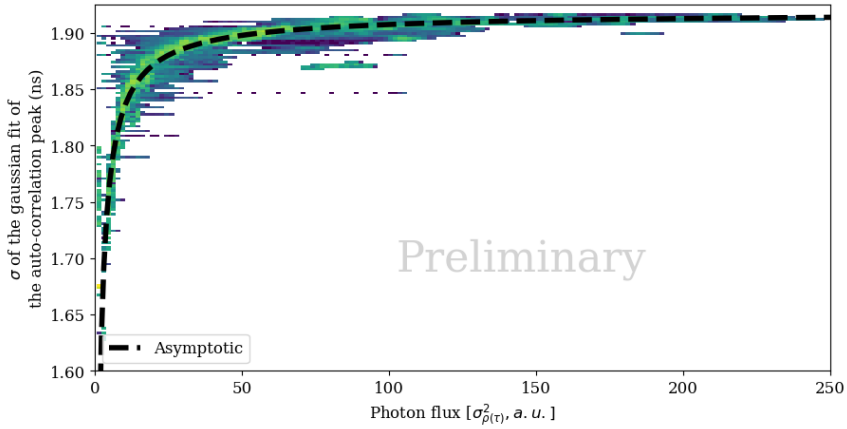

Figure 2: Width of the auto-correlation peak versus different values of photon flux for pixel 251 of the telescope MAGIC 1. A preliminary asymptotic fit is added on top of the 2D density distribution to better visualize the behaviour. For lower photon fluxes the correlation signal is dominated by electronic noise, but for higher fluxes it follows a poissonian.

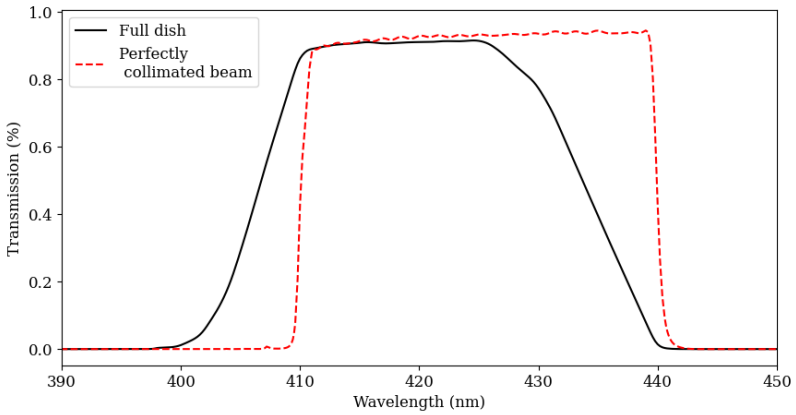

Figure 3: Filter transmission curve for AOIs of 0 deg (perfectly collimated beam) and for the full dish (AOIs from 0 deg to 26 deg), produced with the official tool at https://searchlight.idex-hs.com/ for our Semrock 425-26 nm filters.

Connection problems with the actuators behind each mirror: sometimes the communication is lost between the AMC control and the actuators of the mirrors, resulting in mirrors focused at the position of a previous observation or not focused at all due to other problems with the actuators. This means that the number of mirrors focusing the light into the pixels is not always constant and some light might be missing. MAGIC's AMC allows to keep track of the number of disconnected mirrors, so we can check when this happens. Simulations in which the number of missing mirrors was up to 10 in different locations (random, outer ring, center) showed that this systematic effect is in any case less than 1%.

The weight of the mirror dishes can produce deformations in the overall shape of the dish when pointing at different zenith/azimuth coordinates, changing the distribution of AOIs. This deformation is countered by producing Look Up Tables (LUTs) for the AMC each month that

correct for this effect and maintain the focusing performance in nominal conditions, independent of the zenith/azimuth coordinates.

4.3 Gain of the DC/ADC branch

The gain is the relationship between the number of photo-electrons and the number of electrons that exit the branch. As seen in Eq.4, this value is necessary to properly account for the amount of light that goes into each pixel and to properly compare $DC_{i,Star}$ with $DC_{i,NSB}$, and has a direct effect on the calculation of the contrast and visibility. We have identified several factors that can have an effect on the evolution of the gains, such as: temperature variations, sudden jumps in current that need a few minutes to recover, PMT degradation and changes in high voltage (HV). We perform special HV vs DC calibrations to ensure that changes in $log(HV)$ are proportional to changes in $log(DC)$ for the observed DCs in our nominal set of HV for the pixels. We estimate an overall systematic effect of 1% or less.

4.4 NSB DC subtraction

During interferometry observations we keep track of the NSB in order to properly account for the starlight following Eq.5. We extract $DC_{i,NSB}$ from the 'background pixels' that are not being focused on (up to two in each camera, reserving the third one to observe the star (see picture in Figure 1). Most of the time they receive diffuse light from the Moon. It could happen that a star brighter than the NSB crosses the field of view (FOV) of the background pixels, producing an increase in $DC_{i,NSB}$. This would result in an overestimation of the NSB and a wrong calculation of the contrast and later the visibility. Fortunately, we have two background pixels in each camera when performing full-mirror observations, and can see if one of the $DC_{i,NSB}$ values gets unexpectedly higher than the other. This effect, although occurring in a very small percentage of observations, can be avoided by using the $DC_{i,NSB}$ value from the unaffected background pixel. If this distinction is not made, the effect is in any case less than 3% for stars up to 3.5 B mag.

4.5 Residual electronic noise in the correlation

There is a residual slow noise (one order of magnitude slower than the sampling frequency) coming from the digitizers and correlators that can affect our correlation measurements. When the amount of received photons is very low, the correlation is dominated by this noise, which has a stable shape over time (see Figure 4) and can be easily removed by applying a 12 MHz high-pass filter to the correlation (as stated in section 3). When the amount of received photons is high (i.e. for bright stars) the correlation is no longer dominated by this noise and the effect is much smaller, but we apply the filter in any case.

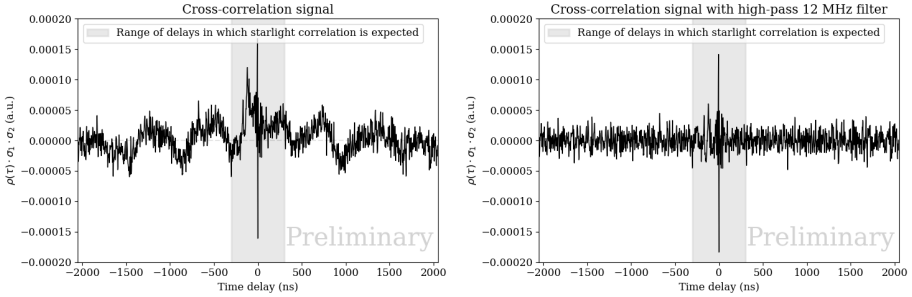

Figure 4: Average of the accumulated cross-correlation data frames in units of $\rho(\tau) \cdot \sigma_1 \cdot \sigma_2$. The total integrated time is over 100 h, for pixel pair MAGIC-1 pixel 251 and MAGIC-2 pixel 251, taken over the course of year 2022. The stable shape of the residual slow electronic noise (left) can be removed by applying a high-pass 12 MHz filter (right). The greyed out zone between ±300 nm is the range of delays in which we typically expect a correlation signal from the star. Within this zone, the shape of the slow electronic noise is intertwined with the stars' correlation signals. After applying the high-pass filter, only the slow noise is subtracted.

5. Conclusions

We have carried out an extensive study of our systematics to ensure that we understand the performance of our interferometer and validate our analysis, which will be presented in detail in an upcoming publication.

References

[1] Abeysekara, A. U., et al. "Demonstration of stellar intensity interferometry with the four VERITAS telescopes." Nature Astronomy 4.12 (2020): 1164-1169.

[2] Acciari, V. A., et al. "Optical intensity interferometry observations using the MAGIC Imaging Atmospheric Cherenkov Telescopes." Monthly Notices of the Royal Astronomical Society 491.2 (2020): 1540-1547.

[3] Aleksić, J., et al. "Performance of the MAGIC stereo system obtained with Crab Nebula data." Astroparticle Physics 35.7 (2012): 435-448.

[4] Aleksić, J., et al. "The major upgrade of the MAGIC telescopes, Part II: A performance study using observations of the Crab Nebula." Astroparticle Physics 72 (2016): 76-94.

[5] Brown, R. H. (1974). The intensity interferometer; its application to astronomy. London.

[6] Brown, R. H., Davis, J., & Allen, L. R. (1974). The angular diameters of 32 stars. Monthly Notices of the Royal Astronomical Society, 167(1), 121-136.

[7] Cortina, J., et al. "First measurements and upgrade plans of the MAGIC intensity interferometer." Optical and Infrared Interferometry and Imaging VIII. Vol. 12183. SPIE, 2022.

[8] Delgado, C., et al. "Intensity interferometry with the MAGIC telescopes." 37th International Cosmic Ray Conference (ICRC 2021). Vol. 395. SISSA, 2021.

Full Authors List: MAGIC Collaboration

H. Abe[1], S. Abe[1], J. Abhir[2], V. A. Acciari[3], I. Agudo[4], T. Aniello[5], S. Ansoldi[6,46], L. A. Antonelli[5], A. Arbet Engels[7], C. Arcaro[8], M. Artero[9], K. Asano[1], D. Baack[10], A. Babić[11], A. Baquero[12], U. Barres de Almeida[13], J. A. Barrio[12], I. Batković[8], J. Baxter[1], J. Becerra González[3], W. Bednarek[14], E. Bernardini[8], M. Bernardos[4], J. Bernete[15], A. Berti[7], J. Besenrieder[7], C. Bigongiari[5], A. Biland[2], O. Blanch[9], G. Bonnoli[5], Ž. Bošnjak[11], I. Burelli[6], G. Busetto[8], A. Campoy-Ordaz[16], A. Carosi[5], R. Carosi[17], M. Carretero-Castrillo[18], A. J. Castro-Tirado[4], G. Ceribella[7], Y. Chai[7], A. Chilingarian[19], A. Cifuentes[15], S. Cikota[11], E. Colombo[3], J. L. Contreras[12], J. Cortina[15], S. Covino[5], G. D'Amico[20], V. D'Elia[5], P. Da Vela[17,47], F. Dazzi[5], A. De Angelis[8], B. De Lotto[6], A. Del Popolo[21], M. Delfino[9,48], J. Delgado[9,48], C. Delgado Mendez[15], D. Depaoli[22], F. Di Pierro[22], L. Di Venere[23], D. Dominis Prester[24], A. Donini[5], D. Dorner[25], M. Doro[8], D. Elsaesser[10], G. Emery[26], J. Escudero[4], L. Fariña[9], A. Fattorini[10], D. Fink[7], M. Fiori[8], L. Foffano[5], L. Font[16], S. Fröse[10], S. Fukami[2], Y. Fukazawa[27], R. J. García López[3], M. Garczarczyk[28], S. Gasparyan[29], M. Gaug[16], J. G. Giesbrecht Paiva[13], N. Giglietto[23], F. Giordano[23], P. Gliwny[14], N. Godinović[30], R. Grau[9], D. Green[7], J. G. Green[7], D. Guberman[17], D. Hadasch[1], A. Hahn[7], T. Hassan[15], L. Heckmann[7,49], J. Herrera[3], D. Hrupec[31], M. Hütten[1], R. Imazawa[27], T. Inada[1], R. Iotov[25], K. Ishio[14], I. Jiménez Martínez[15], J. Jormanainen[32], D. Kerszberg[9], G. W. Kluge[20,50], Y. Kobayashi[1], P. M. Kouch[32], H. Kubo[1], J. Kushida[33], M. Láinez Lezáun[12], A. Lamastra[5], D. Lelas[30], F. Leone[5], E. Lindfors[32], L. Linhoff[10], S. Lombardi[5], F. Longo[6,51], R. López-Coto[4], M. López-Moya[12], A. López-Oramas[3], S. Loporchio[23], A. Lorini[34], E. Lyard[26], B. Machado de Oliveira Fraga[13], P. Majumdar[35], M. Makariev[36], G. Maneva[36], N. Mang[10], M. Manganaro[24], S. Mangano[15], K. Mannheim[25], M. Mariotti[8], G. Martínez[15], M. Martínez[9], M. Martínez-Chicharro[15], A. Mas-Aguilar[12], D. Mazin[1,52], S. Menchiari[34], S. Mender[10], S. Mićanović[24], D. Miceli[8], T. Miener[12], J. M. Miranda[34], R. Mirzoyan[7], M. Molero González[3], E. Molina[3], H. A. Mondal[35], A. Moralejo[9], D. Morcuende[12], T. Nakamori[37], G. Naletto[8], C. Nanci[5], L. Nava[5], V. Neustroev[38], L. Nickel[10], M. Nievas Rosillo[3], C. Nigro[9], L. Nikolić[34], K. Nilsson[32], K. Nishijima[33], T. Njoh Ekoume[3], K. Noda[39], S. Nozaki[7], Y. Ohtani[1], T. Oka[40], A. Okumura[41], J. Otero-Santos[3], S. Paiano[5], M. Palatiello[6], D. Paneque[7], R. Paoletti[34], J. M. Paredes[18], L. Pavletić[24], D. Pavlović[24], M. Persic[6,53], M. Pihet[8], G. Pirola[7], F. Podobnik[34], M. Polo[15], P. G. Prada Moroni[17], E. Prandini[8], G. Principe[6], C. Priyadarshi[9], N. Produit[26], W. Rhode[10], M. Ribó[18], J. Rico[9], C. Righi[5], J. J. Rodríguez-Vázquez[15], P. Saha[2], N. Sahakyan[29], T. Saito[1], S. Sakurai[1], K. Satalecka[32], F. G. Saturni[5], B. Schleicher[25], K. Schmidt[10], F. Schmuckermaier[7], J. L. Schubert[10], T. Schweizer[7], A. Sciaccaluga[5], J. Sitarek[14], V. Sliusar[26], D. Sobczynska[14], A. Spolon[8], A. Stamerra[5], J. Strišković[31], D. Strom[7], M. Strzys[1], Y. Suda[27], T. Surić[42], S. Suutarinen[32], H. Tajima[41], M. Takahashi[41], R. Takeishi[1], F. Tavecchio[5], P. Temnikov[36], K. Terauchi[40], T. Terzić[24], M. Teshima[7,54], L. Tosti[43], S. Truzzi[34], A. Tutone[5], S. Ubach[16], J. van Scherpenberg[7], M. Vazquez Acosta[3], S. Ventura[34], V. Verguilov[36], I. Viale[8], C. F. Vigorito[22], V. Vitale[44], I. Vovk[1], R. Walter[26], M. Will[7], C. Wunderlich[34], T. Yamamoto[45], L. Zampieri[8]

[1] Japanese MAGIC Group: Institute for Cosmic Ray Research (ICRR), The University of Tokyo, Kashiwa, 277-8582 Chiba, Japan
[2] ETH Zürich, CH-8093 Zürich, Switzerland
[3] Instituto de Astrofísica de Canarias and Dpto. de Astrofísica, Universidad de La Laguna, E-38200, La Laguna, Tenerife, Spain
[4] Instituto de Astrofísica de Andalucía-CSIC, Glorieta de la Astronomía s/n, 18008, Granada, Spain
[5] National Institute for Astrophysics (INAF), I-00136 Rome, Italy
[6] Università di Udine and INFN Trieste, I-33100 Udine, Italy
[7] Max-Planck-Institut für Physik, D-80805 München, Germany
[8] Università di Padova and INFN, I-35131 Padova, Italy
[9] Institut de Física d'Altes Energies (IFAE), The Barcelona Institute of Science and Technology (BIST), E-08193 Bellaterra (Barcelona), Spain
[10] Technische Universität Dortmund, D-44221 Dortmund, Germany
[11] Croatian MAGIC Group: University of Zagreb, Faculty of Electrical Engineering and Computing (FER), 10000 Zagreb, Croatia
[12] IPARCOS Institute and EMFTEL Department, Universidad Complutense de Madrid, E-28040 Madrid, Spain
[13] Centro Brasileiro de Pesquisas Físicas (CBPF), 22290-180 URCA, Rio de Janeiro (RJ), Brazil
[14] University of Lodz, Faculty of Physics and Applied Informatics, Department of Astrophysics, 90-236 Lodz, Poland
[15] Centro de Investigaciones Energéticas, Medioambientales y Tecnológicas, E-28040 Madrid, Spain
[16] Departament de Física, and CERES-IEEC, Universitat Autònoma de Barcelona, E-08193 Bellaterra, Spain
[17] Università di Pisa and INFN Pisa, I-56126 Pisa, Italy
[18] Universitat de Barcelona, ICCUB, IEEC-UB, E-08028 Barcelona, Spain
[19] Armenian MAGIC Group: A. Alikhanyan National Science Laboratory, 0036 Yerevan, Armenia
[20] Department for Physics and Technology, University of Bergen, Norway
[21] INFN MAGIC Group: INFN Sezione di Catania and Dipartimento di Fisica e Astronomia, University of Catania, I-95123 Catania, Italy
[22] INFN MAGIC Group: INFN Sezione di Torino and Università degli Studi di Torino, I-10125 Torino, Italy
[23] INFN MAGIC Group: INFN Sezione di Bari and Dipartimento Interateneo di Fisica dell'Università e del Politecnico di Bari, I-70125 Bari, Italy
[24] Croatian MAGIC Group: University of Rijeka, Faculty of Physics, 51000 Rijeka, Croatia
[25] Universität Würzburg, D-97074 Würzburg, Germany
[26] University of Geneva, Chemin d'Ecogia 16, CH-1290 Versoix, Switzerland
[27] Japanese MAGIC Group: Physics Program, Graduate School of Advanced Science and Engineering, Hiroshima University, 739-8526 Hiroshima, Japan

PoS(ICRC2023)728

[28] Deutsches Elektronen-Synchrotron (DESY), D-15738 Zeuthen, Germany
[29] Armenian MAGIC Group: ICRANet-Armenia, 0019 Yerevan, Armenia
[30] Croatian MAGIC Group: University of Split, Faculty of Electrical Engineering, Mechanical Engineering and Naval Architecture (FESB), 21000 Split, Croatia
[31] Croatian MAGIC Group: Josip Juraj Strossmayer University of Osijek, Department of Physics, 31000 Osijek, Croatia
[32] Finnish MAGIC Group: Finnish Centre for Astronomy with ESO, University of Turku, FI-20014 Turku, Finland
[33] Japanese MAGIC Group: Department of Physics, Tokai University, Hiratsuka, 259-1292 Kanagawa, Japan
[34] Università di Siena and INFN Pisa, I-53100 Siena, Italy
[35] Saha Institute of Nuclear Physics, A CI of Homi Bhabha National Institute, Kolkata 700064, West Bengal, India
[36] Inst. for Nucl. Research and Nucl. Energy, Bulgarian Academy of Sciences, BG-1784 Sofia, Bulgaria
[37] Japanese MAGIC Group: Department of Physics, Yamagata University, Yamagata 990-8560, Japan
[38] Finnish MAGIC Group: Space Physics and Astronomy Research Unit, University of Oulu, FI-90014 Oulu, Finland
[39] Japanese MAGIC Group: Chiba University, ICEHAP, 263-8522 Chiba, Japan
[40] Japanese MAGIC Group: Department of Physics, Kyoto University, 606-8502 Kyoto, Japan
[41] Japanese MAGIC Group: Institute for Space-Earth Environmental Research and Kobayashi-Maskawa Institute for the Origin of Particles and the Universe, Nagoya University, 464-6801 Nagoya, Japan
[42] Croatian MAGIC Group: Ruđer Bošković Institute, 10000 Zagreb, Croatia
[43] INFN MAGIC Group: INFN Sezione di Perugia, I-06123 Perugia, Italy
[44] INFN MAGIC Group: INFN Roma Tor Vergata, I-00133 Roma, Italy
[45] Japanese MAGIC Group: Department of Physics, Konan University, Kobe, Hyogo 658-8501, Japan
[46] also at International Center for Relativistic Astrophysics (ICRA), Rome, Italy
[47] now at Institute for Astro- and Particle Physics, University of Innsbruck, A-6020 Innsbruck, Austria
[48] also at Port d'Informació Científica (PIC), E-08193 Bellaterra (Barcelona), Spain
[49] also at Institute for Astro- and Particle Physics, University of Innsbruck, A-6020 Innsbruck, Austria
[50] also at Department of Physics, University of Oslo, Norway
[51] also at Dipartimento di Fisica, Università di Trieste, I-34127 Trieste, Italy
[52] Max-Planck-Institut für Physik, D-80805 München, Germany
[53] also at INAF Padova
[54] Japanese MAGIC Group: Institute for Cosmic Ray Research (ICRR), The University of Tokyo, Kashiwa, 277-8582 Chiba, Japan

PoS(ICRC2023)728